5 Materials Science

5-1 An X-ray Diffraction Study of Layered Nickelate: Commensurate-incommensurate Crossover of Stripe Order

Complex spin-charge-orbital ordering phenomena have been intensively studied as an important topic in the physics of correlated electron systems [1]. Stripe ordering is one example of these phenomena, where doped holes align themselves in one dimension to form a charge-stripe that acts as a domain wall between antiferromagnetic domains (see the inset of Fig. 1). Stripe orderings have been experimentally observed in several systems including high-T_c superconducting cuprates and colossal-magneto resistive manganites, indicating their significant influence on anomalous transport phenomena. Among these systems, layered nickelate $La_{2-x}Sr_xNiO_4$ (LSNO) is a prototypical system showing a firm spin-charge stripe order, especially at $x \sim 1/3$, making it suitable for studying the characteristics of striped states [2].

The charge-stripe order in LSNO is characterized with a modulation vector $q_c = (\varepsilon\ \varepsilon\ 1)$, where the incommensurability ε corresponds to the inverse of the hole-stripe period. ε continuously varies with hole doping while maintaining the relation $\varepsilon \sim x$, reflecting the self-assembly of the doped holes into the half-filled stripes. Recently, however, several diffraction studies have reported upon the temperature (T)-dependence of ε, showing a tendency to deviate from $\varepsilon \sim x$ with increasing T [3,4]. To clarify the origin of such a commensurate-incommensurate (C-IC) crossover of stripe order, we have performed a diffraction measurement using the six-axis spectrometer installed at BL-4C, with a series of LSNO single crystals ($0.25 \leqq x \leqq 0.45$), covering the region around $x \sim 1/3$.

Fig. 1 shows the T-dependence of the superlattice peak profiles along (h h 1) for x = 0.31 (blue traces), 0.333 (black traces), and 0.35 (red traces). The peak corresponds to the reflection at ($2-\varepsilon$ $2-\varepsilon$ 1) due to the charge-stripe order. The sharpest and most symmetric profile is observed for x = 0.333, indicating the special stability of the ε = 1/3 stripe order. The peak positions, which directly reflect the stripe period, are nearly T-independent for x = 0.333 and 0.35. By contrast, for x = 0.31, peak position strongly depends on T, ranging from $\varepsilon \sim 0.325$ at 180 K to 0.305 at 50 K. Such a C-IC crossover is evident over a wide x region, as shown in the $\varepsilon-T$ plot for all the samples [Fig. 2(a)]. The asymmetry between $x < 1/3$ and $x > 1/3$ region, however, is striking. While the T-dependence is very weak for $x \geqq 1/3$, the apparent crossover of incommensurability from $\varepsilon \sim x$ to $\varepsilon \to 1/3$ with increasing T is commonly observed in the lower doped region. This C-IC crossover for $x < 1/3$ may be explained as follows: In the ground state, $\varepsilon \sim x$ is satisfied due to the formation of nearly half-filled hole-stripes (i.e. one-hole per site) as depicted in Fig. 2(c). With increasing T, however, electrons are preferentially be doped into the hole-stripe as shown in Fig. 2(b), leading to the crossover to $\varepsilon \to 1/3$. Actually, the $\varepsilon-T$ curves are well reproduced with a free energy model [5] which takes account the vari-

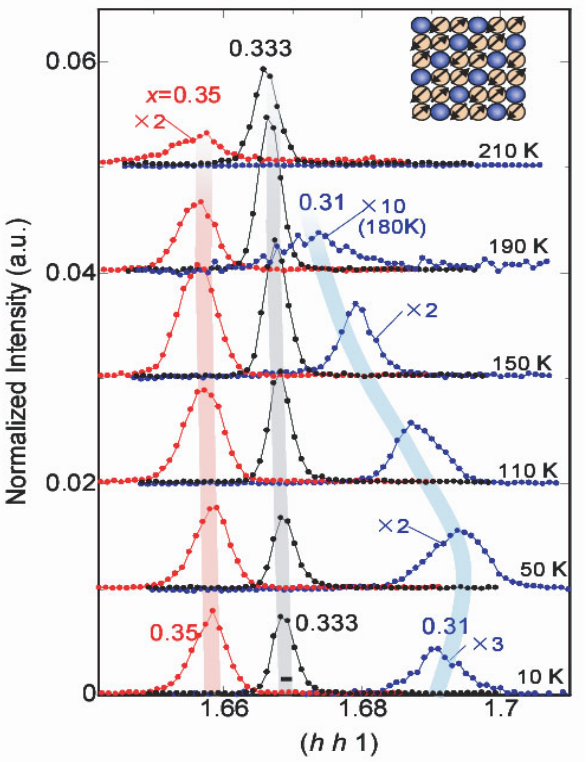

Figure 1
Superlattice profiles at ($2-\varepsilon$ $2-\varepsilon$ 1) due to the formation of the charge stripe order in $La_{2-x}Sr_xNiO_4$ for x = 0.31 (blue), x = 0.333 (black), and x = 0.35 (red). The resolution limit is indicated with a horizontal bar in the 10 K profile for x = 0.333. The inset shows the stripe ordered state at $x = \varepsilon = 1/3$.

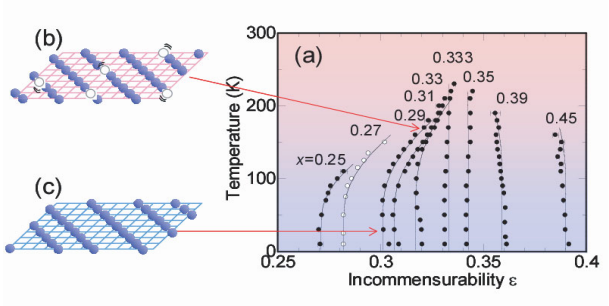

Figure 2
Temperature dependencies of the incommensurability ε of the stripe order for $La_{2-x}Sr_xNiO_4$. The solid curves show the results of a free-energy model analysis [5].

able doping in the stripe, the results of which are shown as solid curves in Fig. 2(a). This indicates that the hole-stripes act as compressible objects against electron-doping, and that the C-IC crossover is a consequence of spontaneous charge transfer between the on- and off-stripe regions, driven by the stability of the ε = 1/3 stripe order together with the entropy effects at high T.

K. Ishizaka[1], T. Arima[2], Y. Murakami[3], R. Kajimoto[4], H. Yoshizawa[1], N. Nagaosa[1,5] and Y. Tokura[1,5] ([1]Univ. of Tokyo, [2]Univ. of Tsukuba, [3]Tohoku Univ., [4]Ochanomizu Univ., [5]AIST)

[1] For review, M. Imada, A. Fujimori and Y. Tokura, *Rev. Mod. Phys.*, **70** (1998) 1039.
[2] H. Yoshizawa, T. Kakeshita, R. Kajimoto, T. Tanabe, T. Katsufuji and Y. Tokura, *Phys. Rev. B,* **61** (2000) R854.
[3] R. Kajimjoto, T. Kakeshita, H. Yoshizawa, T. Tanabe, T. Katsufuji and Y. Tokura, *Phys. Rev. B,* **63** (2001) 144432.
[4] P. D. Hatton, M. E. Ghazi, S. B. Wilkins, P. D. Spencer, D. Mannix, T. D'Almeida, P. Prabhakaran, A. Boothroyd and S. W. Cheong, *Physica B,* **318** (2002) 289.
[5] K. Ishizaka, T. Arima, Y. Murakami, R. Kajimoto, H. Yoshizawa, N. Nagaosa and Y. Tokura, *Phys. Rev. Lett.*, **92** (2004) 196404.

5-2 Time-resolved SAXS Studies on Morphology Formation in Crystalline-Crystalline Diblock Copolymers

Diblock copolymers, consisting of two different blocks covalently connected, form various microdomain structures in the melt depending on their molecular characteristics. When both the blocks are crystalline and their melting temperatures (T_m) differ enough, we can expect a complicated morphology formation when the copolymers are quenched from the melt into low temperatures [1]. It is extremely important to understand the mechanism of such morphology formation when we design new nano-scaled structures with useful properties in polymer materials.

We synthesized various poly(ε-caprolactone)-*block*-polyethylene (PCL-*b*-PE) copolymers, where T_m of the PCL blocks is ca. 58 °C and that of PE blocks is ca. 97 °C. Therefore, the PE blocks crystallized rapidly during quenching to form a lamellar morphology (PE lamellar morphology), an alternating structure composed of lamellar crystals and amorphous layers, and subsequently the PCL blocks crystallized starting from the existing PE lamellar morphology. We have mainly observed the crystallization process of the PCL blocks by using a time-resolved small-angle X-ray scattering (SAXS) method at BL-10C [2].

Fig. 3 shows typical time-resolved SAXS curves recorded during the crystallization of PCL blocks, where the inset represents the thermal history applied to the sample. Immediately after quenching the sample, the sharp SAXS peak turns into a small and diffuse SAXS peak, indicating that the microdomain structure in the melt is immediately transformed into the PE lamellar morphology. After an induction period, the small peak grows with crystallization time, due to the crystallization of PCL blocks. This intensity growth, however, depends significantly on temperature; at low temperatures the peak position does not change at all while at high temperatures it changes discontinuously during crystallization of PCL blocks (Fig. 4). This means that the PE lamellar morphology is not destroyed by the crystallization of PCL blocks at low temperatures and eventually PCL blocks crystallize in the existing PE lamellar morphology. At high temperatures, on the other hand, the crystallization of PCL blocks destroys the PE lamellar morphology to form a new morphology favorable for the crystallization of PCL blocks. This difference in the final morphology formed at lower and higher temperatures was also verified qualitatively by transmission electron microscopy.

In summary, the present results show that the lamellar morphology formed by the first crystallization will be a new class of confinement against the second crystallization in crystalline-crystalline block copolymers. That is, it offers the confinement between the glassy amorphous matrix (hard confinement) and the rubbery matrix (soft confinement usually observed in low molecular weight copolymers), where the degree of confinement would be controlled by changing the volume fraction of pre-existing lamellar crystals.

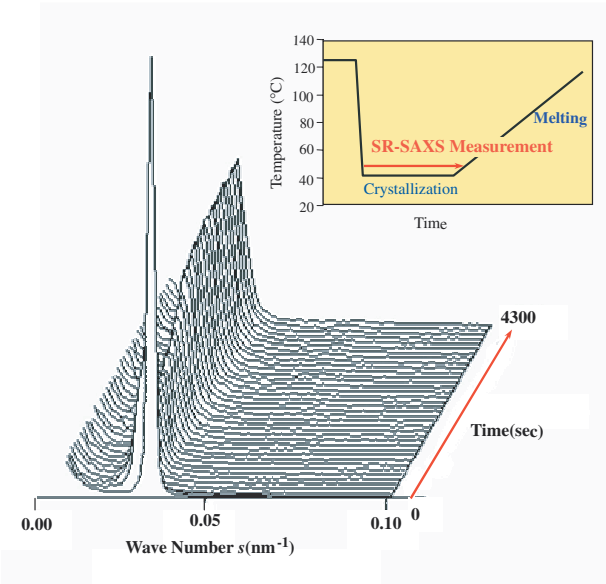

Figure 3
Time-resolved SAXS curves during crystallization of PCL blocks in PCL-*b*-PE. The inset represents the thermal history applied to the sample.

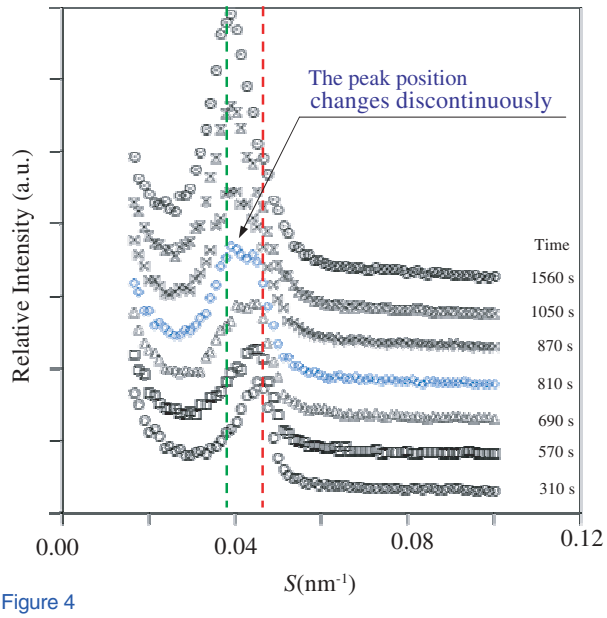

Figure 4
Close investigation of the SAXS curves shown in Fig. 3 as a function of crystallization time *t*. The SAXS curve at *t* = 810 sec shows bimodal character, indicating the coexistence of two morphologies in the system.

S. Nojima (Tokyo Inst. of Tech.)

References

[1] S. Nojima and Y. Akutsu, *Polymer Processing* (in Japanese), **53** (2004) 259.
[2] S. Nojima, Y. Akutsu, A. Washino and S. Tanimoto, *Polymer*, **45** (2004) 7317.

5-3 Magnetic Control of Ferroelectric Polarization

Materials showing both magnetic and ferroelectric orders are called "magnetic ferroelectrics" (recently referred to as *magnetoelectric multiferroics*), in which the coupling between the electric and magnetic polarization is anticipated to give an additional degree of freedom in magnetoelectric and magnetooptical device design. However, there have been few exploratory studies, due to the limited availability of materials and the small magnitude of the effect.

We have discovered gigantic magnetoelectric and magnetocapacitive effects as well as ferroelectricity in some rare-earth manganites [1,2], providing a novel approach to attaining mutual control between magnetism and ferroelectricity. The rare-earth manganites we investigated ($TbMnO_3$ and $DyMnO_3$) have an orthorhombically distorted perovskite structure (with space group *Pbnm*) at room temperature, and show a sinusoidal antiferromagnetic ordering of the Mn^{3+} moments below T_N~40 K with a wave vector q = (0,k_s,1). Crystallographic and magnetic structures for $TbMnO_3$ are illustrated in Fig. 5(a). At lower temperatures (T_C), ferroelectric order with spontaneous polarization along the *c* axis appears, as shown in Fig. 6(d).

X-ray diffraction measurements at BL-4C have revealed the lattice distortion producing the polar structures and the relationship between magnetism and ferroelecricity in the rare-earth perovskite manganites [1,3]. Figs. 6(a) and 6(b) show X-ray diffraction scans along (0,*k*,3) at various temperature for $TbMnO_3$ and $DyMnO_3$ crystals. For both crystals, additional superlattice peaks appear at the wave vector (0,k_l,*l*) for integer *l* at temperature below T_N. Fig. 6(c) shows the temperature dependence of wave number k_l and normalized intensity of superlattice reflection at (0,k_l,3) attributed to the lattice modulation. For both $TbMnO_3$ and $DyMnO_3$, k_l is temperature-dependent just below T_N, but is locked-in below T_C [Fig. 6(c)]. The value of k_l is almost twice as large as that of k_s, as illustrated in Fig. 5(b). It is well-known that crystallographic deformations at magnetic ordering are due to the exchange striction. The observed superlattice reflections due to the atomic displacement can be regarded as the second harmonic peaks magnetoelastically induced by sinusoidal antiferromagnetic order.

The close relationship between lattice modulation and ferroelectricity is common to the so-called improper ferroelectrics (e.g. K_2SeO_4, Rb_2ZnCl_4), where the primary order parameter represents the lattice distortion mode

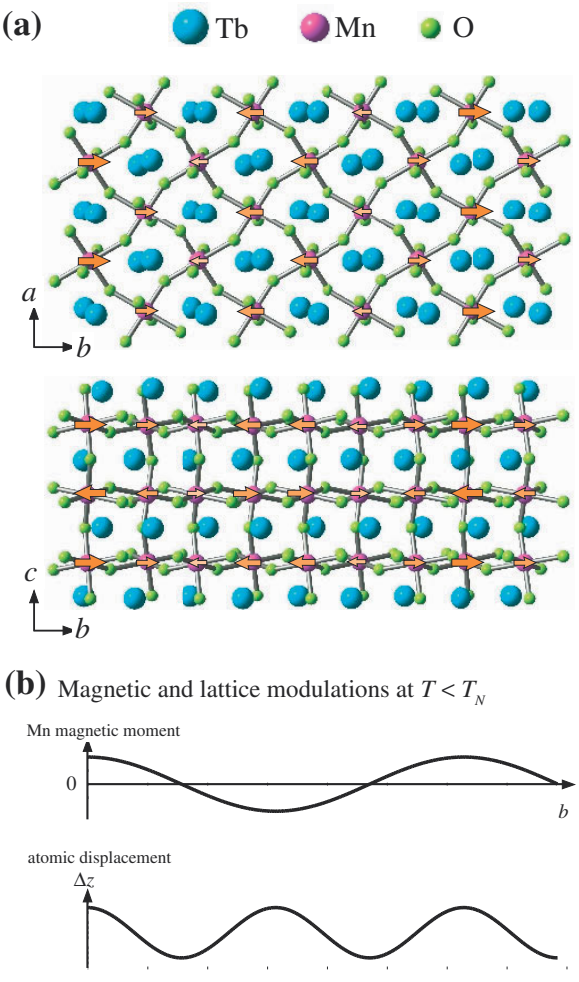

Figure 5
(a) Sketches of crystal structure at room temperature and (b) spatial variation along the *b*-axis of Mn magnetic moment and atomic displacement (Δz//*c*) below T_N in $TbMnO_3$. Orange arrows denote Mn magnetic moments below T_N.

having nonzero wave vector (that is $k_l \neq 0$), and the spontaneous polarization appears as a secondary order parameter induced by the lattice distortion. This may also be the case for the perovskite rare-earth manganites.

These observations show that the ferroelectricity in these manganites ordinates in magnetic interactions, through magnetoelastically-induced lattice modulations. Supporting this view, we observed a fascinating magnetoelectric coupled phenomenon, which we call "magnetic-field induced electric polarization flop" [1,2], where the direction of the ferroelectric polarization can be switched from the *c* to the *a* axis by the application of a magnetic field [inset of Fig. 6(d)]. These results provide a path to new magneto-electric applications.

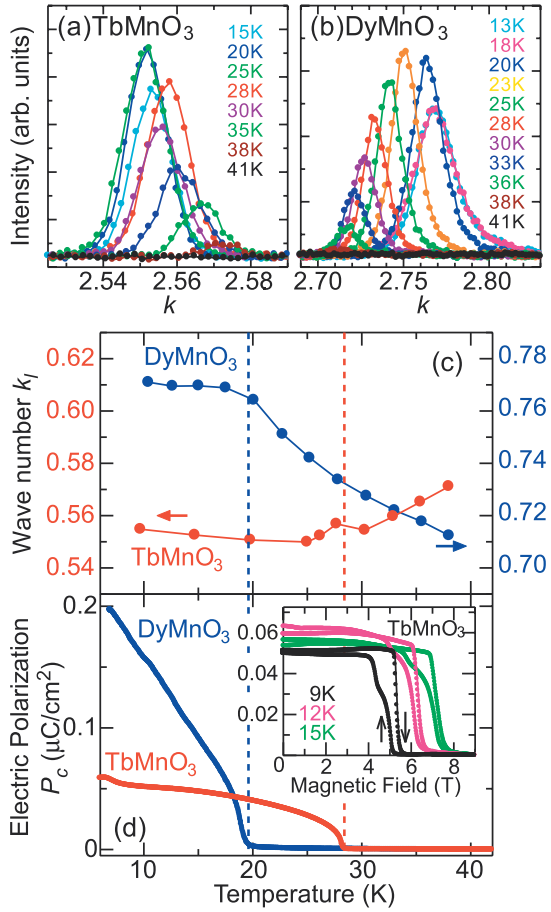

Figure 6
X-ray diffraction *k*-scans along (0,*k*,3) at various temperatures for single crystals of (a) $TbMnO_3$ and (b) $DyMnO_3$. Temperature profiles of (c) wave vector of lattice modulation k_l and (d) electric polarization along the *c* axis in single crystals of $TbMnO_3$ and $DyMnO_3$. The dashed lines denote the lock-in (ferroelectric) transition temperature. Inset: Electric polarization along the *c* axis as a function of magnetic field at selected temperatures for $TbMnO_3$.

T. Kimura[1], T. Arima[2] and Y. Tokura[3] ([1]Los Alamos National Laboratory, [2]Tohoku Univ., [3]Univ. of Tokyo)

References

[1] T. Kimura, T. Goto, H. Shintani, K. Ishizaka, T. Arima and Y. Tokura, *Nature* (London), **426** (2003) 55.
[2] T. Kimura, S. Ishihara, H. Shintani, T. Arima, K. T. Takahashi, K. Ishizaka and Y. Tokura, *Phys. Rev. B,* **68** (2003) 060403(R).
[3] T. Goto, T. Kimura, G. Lawes, A. P. Ramirez and Y. Tokura, *Phys. Rev. Lett.*, **92** (2004) 257201.

5-4 An X-ray Micro Diffraction Analysis of the Dynamic Local Layer Response to an Electric Field in Ferroelectric Liquid Crystals

Liquid crystal research has become an interdisciplinary field having practical applications. Among the various phases of liquid crystals, the smectic C (SmC) phase is characterized by a one-dimensional order and that a rod-like molecule tilts with respect to the layer normal. Ferroelectricity in liquid crystals was first observed in the chiral SmC* phase followed by the discovery of its fast electro-optic switching. In the last ten years, antiferroelectricity and intermediate ferrielectric phases have been found and systematic research into the chiral smectic phase of (anti-)ferroelectric liquid crystals [(A)FLCs] has been intensively performed, though the origin of these phases is still unclear. In order to understand the electro-optical response of the (A)FLC, analysis of the static and dynamic layer structure in an electric field is crucial. Since the SmC* phase in an electric field shows a characteristic texture observable by an optical microscope, X-ray microbeams are indispensable for its study. Recently, time-resolved synchrotron X-ray micro-diffraction has been applied to the characterization of the local layer structure of the SmC* phase, revealing the dynamic as well as the static layer structure [1].

BL-4A was used for the micro-diffraction experiment (3 × 4 μm^2 focus size). The diffracted intensities were measured as a function of angles ω and χ, which correspond to the layer orientation with respect to the rubbing direction normal and the surface normal, respectively. Time resolved measurements were performed with a time resolution of a few μs. The samples were homogeneously aligned TK-C101 (FLC, Chisso) sandwiched between Indium Tin Oxide (ITO)-coated glass plates, and the cell gap was 7.5 μm.

The irreversible layer transformation under increasing electric field consisted of two stages. With an applied field of AC the initial vertical-chevron (v-chevron) structure transformed to an alternating vertical and horizontal chevron structure [Fig. 7(a)]. Further increasing the field, the chevron angle decreased and a horizontal chevron (h-chevron) structure developed [Fig. 7(b) and (c)]. Corresponding optical micrographs show the generation [Fig. 7(d)], development [Fig. 7(e)] and the modification [Fig. 7(f)] of the stripe texture. The time-resolved micro-diffraction measurement has clarified the detailed reversible layer transformation. Figs. 8(a) and (b) show the time resolved ω- and χ-profiles for the triangular wave form applied field. At low voltage, the ω- and χ-profile shows a double peak. At high voltage, a single peak appears in the ω-profile while a double peak with a relatively large angular separation is seen in the χ-profile. Since the profile changes periodically from position to position,

it is concluded that the local layer transforms between a mostly h-chevron with a small portion of the v-chevron structure at high field [Fig. 8(c)] and the so-called quasi-bookshelf structure at the low field. This layer transformation can be explained in terms of the electric torque and surface anchoring. At high field, the electric torque due to the interaction between the electric field and the spontaneous polarization makes the layer upright, while surface anchoring due to the rubbed alignment film tends to form the v-chevron structure. The local layer structure at high field is due to the competition between these two forces. The transient response time of the local layer for the square wave form was measured for the first time. The layer responds to the external field quickly within 0.1~0.4 ms; this was found to be slightly longer than the optical response time.

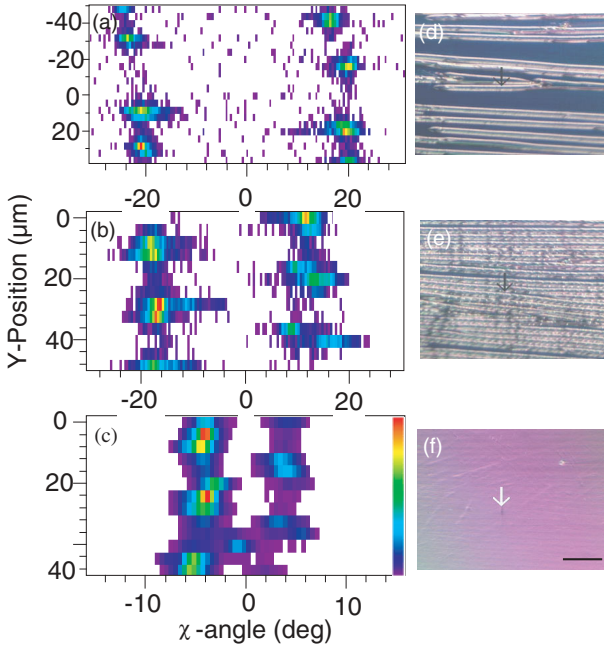

Figure 7
Series of χ-profiles (a)~(c) and corresponding polarized optical micrographs of FLC texture (d)~(f) under an AC electric field. Applied voltages are ±18 V (a) and (d), ±30 V (b) and (e), and ±60 V (c) and (f). A scale mark in (f) represents 100 μm.

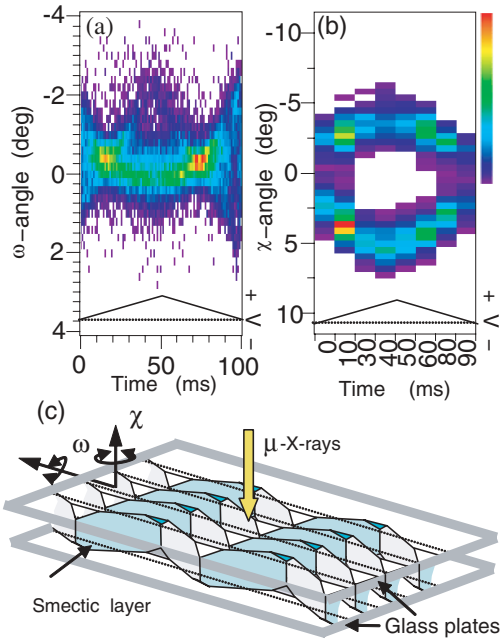

Figure 8
Time resolved ω-profiles (a) and χ-profiles (at ω ~ 0°) (b) for a half cycle of the applied triangular wave form electric field (5 Hz, ±60V). The lower insets show the applied wave form. (c) A schematic representation of the possible local layer structure at high electric field.

Y. Takahashi[1] and A. Iida[2] ([1]Nihon Univ., [2]KEK-PF)

Reference

[1] Y. Takahashi, A. Iida, Y. Takanishi, T. Ogasawara, M. Nakata, K. Ishikawa and H. Takezoe, *Phys. Rev. E,* **67** (2003) 051706.